

Fast and Robust Bio-inspired Teach and Repeat Navigation

Dominic Dall’Osto, Tobias Fischer and Michael Milford

Abstract—Fully autonomous mobile robots have a multitude of potential applications, but guaranteeing robust navigation performance remains an open research problem. For many tasks such as repeated infrastructure inspection, item delivery or inventory transport, a route repeating capability rather than full navigation stack can be sufficient and offers potential practical advantages. Previous teach and repeat research has achieved high performance in difficult conditions generally by using sophisticated, often expensive sensors, and has often had high computational requirements. Biological systems, such as small animals and insects like seeing ants, offer a proof of concept that robust and generalisable navigation can be achieved with extremely limited visual systems and computing power. In this work we create a novel asynchronous formulation for teach and repeat navigation that fully utilises odometry information, paired with a correction signal driven by much more computationally lightweight visual processing than is typically required. This correction signal is also decoupled from the robot’s motor control, allowing its rate to be modulated by the available computing capacity. We evaluate this approach with extensive experimentation on two different robotic platforms, the Consequential Robotics Miro and the Clearpath Jackal robots, across navigation trials totalling more than 6000 metres in a range of challenging indoor and outdoor environments. Our approach is more robust and requires significantly less compute than the state-of-the-art. It is also capable of intervention-free – no parameter changes required – cross-platform generalisation, learning to navigate a route on one robot and repeating that route on a different type of robot with different camera.

I. INTRODUCTION

Visual navigation is a key capability for mobile robots to operate in a large range of environments without needing dedicated infrastructure – vision being the primary sense humans use for navigating our world [1]. Navigation approaches are chiefly characterised by whether they use a map, and whether the map is metrically consistent or provides only topological information [2]. A general solution to the navigation problem remains illusive, but useful behaviours have been developed for limited ranges of conditions or environments.

Repeated route following is a useful capability for a mobile robot in many different applications: for a tour guide robot in a museum [3], for a drone conducting environmental inspection [4], for automated mining transport trucks [5], or for an interplanetary rover repeatedly collecting samples. By considering that the robot only needs to traverse predetermined paths within the environment, the navigation

The authors are with the QUT Centre for Robotics, Queensland University of Technology, Brisbane, QLD 4000, Australia (e-mail: dominic.dallosto@qut.edu.au). This work received funding from the Australian Government, via grant AUSMURIB000001 associated with ONR MURI grant N00014-19-1-2571. All authors acknowledge continued support from the Queensland University of Technology (QUT) through the Centre for Robotics.

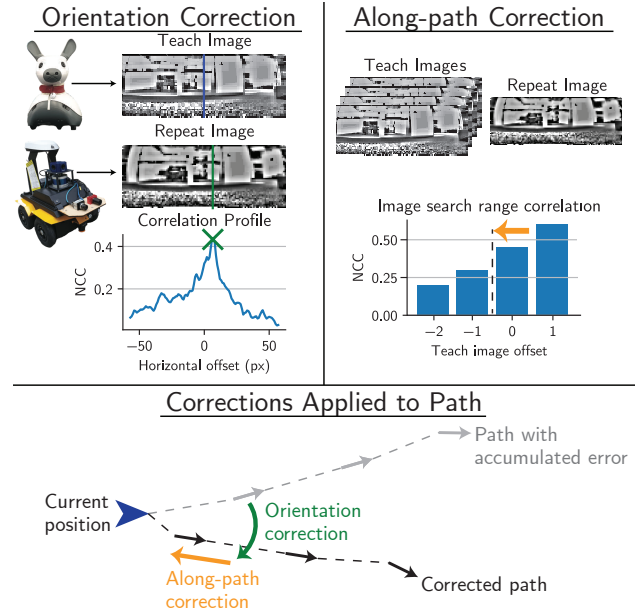


Fig. 1. Overview of our approach: Our teach and repeat system is predominantly driven by wheel odometry, with orientation and along-path corrections made using visual information. This framework enables fast and robust teach and repeat navigation, even in challenging situations like the teach and repeat runs being performed on very different robotic platforms (e.g. Miro and Jackal).

problem can be solved by the teach and repeat framework [6]–[9]. Here, the robot is first manually driven along a route of interest while recording data. The recorded information is then used to robustly repeat this same route.

Teach and repeat has been proven a robust and flexible in many domains, from simple indoor environments [10]–[14] to the surface of another planet [9], [15], [16]. But even low compute teach repeat methods [10] still require high resolution images and significant computation for feature detection. This limits their deployment on small low-cost robots, for which a simple route following capability would be most useful. Such robots do not typically have stereo vision or LiDAR sensors. In contrast, almost all mobile robots have wheel odometry sensors and a monocular camera.

Our chief contribution in this work is a teach and repeat system that is predominantly driven by wheel odometry, with vision only providing a periodic correction signal. This allows us to reduce the complexity of the image processing needed to compute a reliable correction. Additionally, it allows decoupling the robot’s basic navigation from the visual input, so the correction rate can be changed as dictated by the available computation. This approach is verified experimentally with numerous navigation trials totalling

more than 6000 metres on two different robotics platforms in different environments. Notably, our approach can be deployed to new robots with minimal tuning, and indeed the teach run from one robot can be repeated on another. We also show this approach is very robust to errors in the odometry information on which it relies. An overview of our approach is shown in Figure I.

The body of this paper proceeds as follows. In Section II, we present related work from the field of teach and repeat and visual navigation. In Section III we detail the novel aspects of our approach. In Section IV we present details of our experiments and their results. Finally, in Section V we provide conclusions from this work and detail avenues for future work.

II. RELATED WORKS

Teach and repeat navigation falls under the broader capability of route following, which we briefly review in Section II-A. We then provide an overview of teach and repeat navigation approaches in Section II-B.

A. Route Following

Route following approaches for mobile robots are most easily distinguished by the types of map they use for navigation: metric; topological; or a hybrid of the two called topometric. We will introduce these three approaches in the following subsections, and provide some key references to relevant works.

1) *Metric Map*: A robot could explore and build an accurate metric map of the environment (as in Simultaneous Localisation and Mapping [17]), and then use this map to track its location and repeat the desired route. A metric map allows for the most accurate route repetition, but maintaining a metrically consistent map scales in computational complexity with the size of the environment, so it is not commonly applicable to low-cost robots. Many robot navigation behaviours are still possible without a metric map [2]. Indeed, it has recently been proven that local correction signals at each point along the path are sufficient for route following [6].

2) *Topological Map*: Visual homing is an approach where a robot's goal is expressed as an image and the robot moves through the world to reach this location, without considering the world's geometry. Simple visual homing techniques are exhibited by ants and other insects to return to food or nesting sites [18], [19]. Visual homing can be extended for route following by using a topological map of the route – considering the route as a sequence of visual goals and updating the current goal whenever the previous one is reached.

However, visual homing techniques do not guarantee a smooth trajectory straight towards the goal [20]. A sequential route representation is only minimally robust, because failing to reach any goal due to lighting changes or occlusion cause the route following to fail completely. Indeed, recent research debates whether ants combine path integration of their movements with visual information to form a cognitive map, enabling more robust homing behaviours [21].

3) *Topometric Map*: An alternative formulation is a topometric map, where locally accurate movement information such as wheel or visual odometry is combined with globally accurate sensor readings from a camera or LiDAR to form a map that is only *locally* consistent. By not enforcing global consistency, topometric maps can efficiently scale to large environments. Route following is then achieved through the teach and repeat technique. In the teach portion the robot is driven once along the desired route, storing a series of sensory information. In the repeat run the robot then follows the trained route, robust to slight deviations from the path or variations in the environment.

B. Teach and Repeat Navigation

Early work on teach and repeat showed that following a route was possible by only making heading corrections along that route, without requiring a consistent map [22], [23]. Further work developed a provably convergent control rule for this formulation [24]. Krajnik et al. [10] have proven teach repeat stable for a closed polygonal path, extended to arbitrary routes in [6].

Teach and repeat has also been employed in various domains: it has enabled autonomous navigation and emergency return capabilities for unmanned aerial vehicles in GPS denied environments [7], [8], and has also been used for autonomous underwater vehicles to repeat previous routes using sidescan sonar imagery [25], [26]. But in the following subsections we focus exclusively on teach and repeat for mobile robots, categorising approaches by the way they compare images between the teach and repeat runs.

1) *Direct visual methods*: The simplest approach is direct visual comparison, where full images are compared between the teach and repeat runs. These techniques can generally be run with lower resolution images so need the least computation, however they can be less robust to appearance change or large shifts in image location.

This can be ameliorated by image preprocessing techniques, and by assuming the robot's environment is flat so displacements will only occur horizontally in the image. For example, [22] used cross correlation to find the horizontal offset between teach and repeat images, providing the error signal for correction.

Similarly, optimising the mutual information between reference and query images has been used to formulate a teach and repeat control rule that is robust to occlusion and lighting variations [11], [27].

2) *Feature based methods*: In contrast to direct comparison methods, feature based techniques extract a number of salient features – generally points, edges or corners – from each image, and compare these between teach and repeat runs. Corresponding point locations can be used to estimate the geometrical offset between matched images. While typically more computationally intensive and with limitations in featureless environments, feature based comparison methods are the most widely used for teach and repeat. Early work derived a control scheme from the horizontal location of

feature correspondences in monocular images [28], which was later made more robust by incorporating wheel odometry [29].

To improve performance in challenging lighting conditions, depth images rendered from LiDAR scans were adopted in [15]. Furthermore, the approach was modified for monocular cameras in [16], where the assumption of a flat ground plane allowed recovering depth information from single images.

The feature based approach to teach and repeat approach has recently been extended with work from the visual place recognition field (see Lowry et al. [30] for a survey), where more detailed image descriptors are used to uniquely identify images in the world. For example, [14] used image descriptors that are generated by a Convolutional Neural Network. This has the added benefit of being much more robust to appearance and viewpoint changes. Similarly, [12] presented a purely visual teach and repeat approach using image line features, as they are more robust to occlusion and motion blur. [13] extended this to a hybrid approach using both line and point features.

III. PROPOSED APPROACH

This work reformulates the provably convergent teach and repeat correction rule from [24] in a geometric framework, so odometry information from the reference run can be more efficiently used when the route is repeated. The reformulation expresses each waypoint in the route as a pose relative to the robot’s odometry frame. This approach decouples odometry information from the visual information stream so that the robot can be smoothly controlled at high frequencies with a lower rate image correction, allowing for reduced computation and graceful performance degradation. Here we detail the approaches to the two distinct phases of operation for the robot: teach and repeat. To foster future research on our approach, we make the code available for research purposes¹.

The following notation is used: Poses are denoted by boldface lowercase symbols, such as \mathbf{p} for the robot’s pose and \mathbf{g} for the goal pose. Poses with a hat, such as $\hat{\mathbf{p}}$, are in the robot’s local reference frame with respect to odometry, while poses without, such as \mathbf{p} , are in a globally consistent reference frame.

A. Teach phase

In the teach phase the robot is manually teleoperated along the desired route, while recording a list of associated odometry poses and images. As the odometry information suffers from drift and is not globally consistent, this results in a topometric map of the route. This topometric map, \mathbf{R} , consists of an ordered list of pairs of 3 degrees-of-freedom odometry poses, \mathbf{g} , and images, \mathbf{I} , of cardinality N .

$$\mathbf{R} = \{(\mathbf{g}_1, \mathbf{I}_1), (\mathbf{g}_2, \mathbf{I}_2), \dots, (\mathbf{g}_N, \mathbf{I}_N)\} \quad (1)$$

A new entry $(\mathbf{g}_{N+1}, \mathbf{I}_{N+1})$ was appended to the route whenever the displacement of the robot from the last recorded pose exceeded a certain distance τ_d or angular threshold

τ_α . Lower thresholds allowed for denser maps and more accurate path following at the expense of a greater memory requirement.

Image Processing: Before being saved, the images are preprocessed by downscaling them, converting to greyscale, and applying patch normalisation. Downscaling significantly reduces the memory required to store the route, and patch normalisation [31] affords the system robustness to lighting variation.

B. Repeat phase

In the repeat phase, the robot reads from the topometric map and uses the stored data to best follow it. Control of the robot is separated hierarchically, with a low level odometry-based controller driving the robot to a nearby pose in its odometry frame, $\hat{\mathbf{g}}$ (see Section III-B.1), and a route correction controller updating the target pose based on the current image frame, $\hat{\mathbf{I}}$. These corrections are computed separately for orientation – accounting for heading and lateral path errors (see Section III-B.2) – and along-path errors (see Section III-B.3).

1) *Odometry driven control:* The odometry-based controller receives a high frequency estimate of the robot’s pose from integrated wheel odometry information, $\hat{\mathbf{p}}$, and controls the robot’s motors so it reaches a goal pose, $\hat{\mathbf{g}}$. Both of these poses are expressed in the robot’s local odometry frame.

A pose controller, detailed in [32], calculates the motor velocities based on the offset between the current pose and the goal. This controller was modified so the robot could not reverse, and a turn-on-the-spot routine was added and triggered if the goal was behind the robot, or if the robot reached the goal position facing the wrong direction.

2) *Image based orientation correction:* Incoming images, $\hat{\mathbf{I}}$, are pre-processed as described for the teach run (see Section III-A). Normalised Cross Correlation (NCC) [33] is used to compare the incoming images to those saved during the teach run, \mathbf{I} . Assuming that the robot operates on a flat ground plane, rotational and lateral offsets from the path both cause a horizontal image displacement. Without depth information, these two errors are indistinguishable. However, as they both elicit the same correction response, our approach considers them in the same manner. Specifically, the query image is swept horizontally over a search range, $d \in [-D, D]$, and the NCC computed with the reference image for each of these offsets:

$$\text{NCC}_d(\mathbf{I}, \hat{\mathbf{I}}) = \frac{\sum_{x,y} [\mathbf{I}(x, y) - \bar{\mathbf{I}}_d] [\hat{\mathbf{I}}(x - d, y) - \bar{\hat{\mathbf{I}}}_d]}{\left\{ \sum_{x,y} [\mathbf{I}(x, y) - \bar{\mathbf{I}}_d]^2 \sum_{x,y} [\hat{\mathbf{I}}(x - d, y) - \bar{\hat{\mathbf{I}}}_d]^2 \right\}^{0.5}}, \quad (2)$$

where $\bar{\hat{\mathbf{I}}}$ is the mean of the query image and $\bar{\mathbf{I}}_d$ is the mean of the reference image in the valid area overlapping the query image shifted by d pixels. The offset with the greatest NCC,

$$\delta(\mathbf{I}, \hat{\mathbf{I}}) = \arg \max_d (\text{NCC}_d(\mathbf{I}, \hat{\mathbf{I}})), \quad (3)$$

¹<https://github.com/QVPR/teach-repeat/>

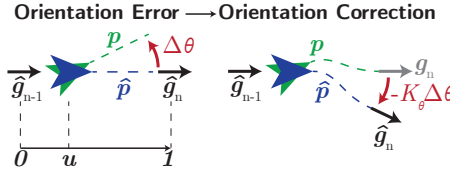


Fig. 2. Overview of orientation correction: An error between the robot's estimated pose, \hat{p} , and actual pose, p , is calculated by interpolating the image offsets between the previous goal, \hat{g}_{n-1} , and current goal, \hat{g}_n , using interpolation factor, u . This error, $\Delta\theta$, is multiplied by a gain factor, K_θ , to rotate the target path so the robot correctly follows the taught route.

is used as the offset estimate. Knowing the resolution and horizontal field of view of the image, this pixel offset is converted to an offset angle, θ_δ .

Following [24], image offsets are interpolated between the previous and next goals to allow for corrections to be made continually between goal locations. Being in front of or behind a goal could induce an image offset in either direction, depending on the dominant visual features in the scene. An object on the left will appear to move further left if the robot moves forwards, while an object on the right will appear to move right. Interpolating the offset between goals cancels out this along-path induced offset, allowing it to be distinguished from rotational or lateral path offsets, which affect both δ_{n-1} and δ_n similarly.

The interpolation factor, u , is the proportion of the distance travelled between two keyframe poses. Specifically, u can be calculated with odometry information as follows:

$$u = \frac{(\hat{g}_n \ominus \hat{g}_{n-1}) \cdot (\hat{p} \ominus \hat{g}_{n-1})}{\|\hat{g}_n \ominus \hat{g}_{n-1}\|^2}, \quad (4)$$

where \hat{p} is the robot's pose estimate, and \hat{g}_n is the pose of keyframe n in the robot's odometry frame (see Figure III-B.2). \ominus denotes pose subtraction, \cdot denotes the dot product of two poses, and $\|\mathbf{x}\|$ denotes the vector magnitude of pose \mathbf{x} .

The orientation offset of the robot from the path at this point between the two keyframes is interpolated as follows:

$$\Delta\theta = (1 - u)\theta_{\delta,n-1} + u\theta_{\delta,n}, \quad (5)$$

where $\theta_{\delta,n}$ is the rotational offset to keyframe n . To correct this error, the current goal pose is rotated about the robot in the opposite direction to the visual offset:

$$\hat{g}_n := \hat{p} \oplus \mathcal{R}_{(-K_\theta \Delta\theta)}(\hat{g}_n \ominus \hat{p}), \quad (6)$$

where $\mathcal{R}_\theta(\mathbf{x})$ is a transformation that rotates pose \mathbf{x} by angle θ , K_θ is a calibrated gain term, and \oplus denotes pose addition.

3) *Image based along-path correction:* In addition to lateral or rotational errors, the robot can have an offset from travelling too quickly or slowly along the path. For this case, the assumption was made that NCC values would be strongest for images closest to the current location. A small search range, $\pm K$, was centred on the previous and current goals images, i.e. I_{n-2} to I_{n+1} for $K = 1$, and correlation values compared for this range. Higher correlation values ahead of the robot pull it forwards along the path, and vice versa. This

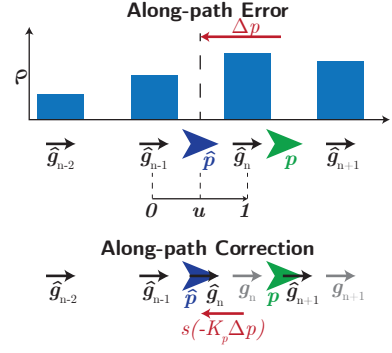


Fig. 3. Overview of along-path correction: An error between the robot's estimated pose, \hat{p} , and actual pose, p , is calculated by finding the goal, \hat{g}_n , with the image that correlates most strongly, ρ , to the current image, relative to u . This error, Δp , is multiplied by a gain factor, K_p , converted to a scaling parameter, s , and used to extend or retract the target path so the robot correctly follows the taught route.

provides incremental corrections to account for random and systematic odometry errors. For goals at the start or end of the route where the full search range is not valid, the search range is symmetrically scaled down to fit.

Peak correlations between the query and reference images over the search range are weighted and averaged to compute an estimate of the robot's along path error, Δp , as follows:

$$\rho = \max \left(\text{NCC}_d(I_n, \hat{I}) \right) \forall n \in [-(K+1), K] \quad (7)$$

$$\hat{p} = \frac{\max(\rho - 0.1, 0)}{\sum \max(\rho - 0.1, 0)} \quad (8)$$

$$\Delta p = \sum_{n=-(K+1)}^K (n\hat{p}_n) - u, \quad (9)$$

Where NCC_d is defined in Eq. (2) and u is defined in Eq. (4). This position estimate is in units of goal spacing, τ_d , so is converted to a scaling correction factor, s , for the current goal:

$$s = \frac{\|\hat{g}_n \ominus \hat{p}\| - K_p \Delta p \tau_d}{\|\hat{g}_n \ominus \hat{p}\|} \quad (10)$$

$$\hat{g}_n := \hat{p} \oplus s(\hat{g}_n \ominus \hat{p}), \quad (11)$$

where K_p is a calibrated gain term, and τ_d is defined in Section III-A.

If the correlation values are higher for images behind the robot's estimated location, i.e. $\Delta p < 0$, such that $s > 1$, the current goal will be extended, giving the true pose, p , time to "catch up" to the estimated pose, \hat{p} . The opposite case occurs if the robot estimates its position to be behind its true pose. A visualisation of the along-path correction is provided in Figure III-B.3.

4) *Global Initialisation:* When starting to repeat, the NCC (Eq. 2) is computed for all images in the route and the best match selected as the starting point. This allows the robot to localise to within $\frac{\tau_d}{2}$ of its true pose, ensuring robust route following as this distance is within the along-route search range, K . But if the NCC is below a threshold, the robot can detect that it is not located along the route and so does not start route repetition.

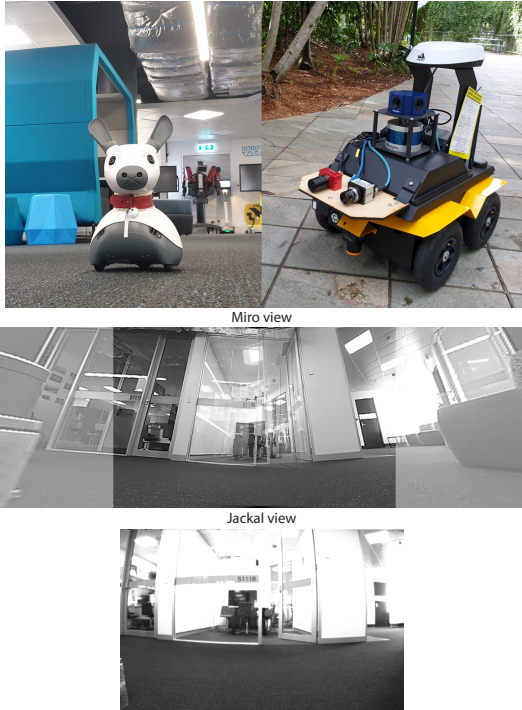


Fig. 4. (Top) Robotic platforms considered in this paper: Miro traversing the indoor route (left) and Jackal traversing the outdoor route (right). The front facing camera from the blue omnidirectional camera was used on the Jackal. For the Miro, images from the two eyes were stitched together into one with some distortion artefacts. (Bottom) Example views from Miro and Jackal. Miro's view was cropped to approximately match that of Jackal when transferring the teach run between robots as described in Section IV-D.

IV. EXPERIMENTAL RESULTS

In this Section, we first outline the experimental procedure and the two robotic platforms used in Section IV-A. This is followed by a set of comprehensive indoor trials in Section IV-B, showing that our approach is robust to odometry errors, is not sensitive to path correction gain parameter values, and works with images of a very low resolution. In Section IV-C we briefly demonstrate that our approach can be applied outdoors (550 m route) at different times of the day and in varying weather conditions (4 repeat runs one month after the teach run). Finally, Section IV-D discusses the challenges of recording a teach run on the Miro robot and repeating that run on the Jackal, whereby the camera, viewpoint and odometry significantly differ between the platforms.

A. Experimental Procedure

The proposed teach repeat system was run on the Jackal and Miro robots (Figure 4) in both indoor and outdoor environments (also see our Multimedia Material). All robot parameters were set as shown in Table I unless otherwise specified. We want to note that the same parameters were used indoors and outdoors, and only a single parameter (τ_d) differed between the two robot platforms (however τ_d was set to the same value on both platforms in Section IV-D without any loss in performance).

We used the Jackal's Velodyne LiDAR sensor to run SLAM [34], so we were able to measure how closely the

TABLE I
PARAMETER VALUES FOR THE TWO ROBOTIC PLATFORMS

Image Processing		
Parameter	Jackal value	Miro value
Image size	115×44	115×44
Patch normalisation size	9×9	9×9
NCC search range, D (px)	± 75	± 75
Image horizontal FOV ($^{\circ}$)	75	175.2
Teach		
Parameter	Jackal value	Miro value
Distance threshold, τ_d (m)	0.3	0.2
Angle threshold, τ_{α} ($^{\circ}$)	15	15
Repeat		
Parameter	Jackal value	Miro value
Orientation correction gain, K_{θ}	0.01	0.01
Along-path correction gain, K_p	0.01	0.01
Along-path search range, K	3	3

repeat run matched with the teach run. It must be emphasised that this SLAM process was run entirely independently from our teach and repeat approach – no information was shared between them. Although not providing real ground truth information, SLAM was deemed to be suitably accurate to allow metric error analysis indoors. In the outdoor trials, relatively large relocalisation jumps occurred, so these data are only used as a visualisation.

Additionally, we present comparison results against a state-of-the-art benchmark system, Bearnav [6]. Bearnav is to the best of the authors' knowledge the only open-source teach and repeat method, and has recently been used as a comparison method in [14].

B. Indoor Comprehensive Trials

These experiments were performed on the Jackal robot in an office environment for which a high resolution SLAM map was already available, to enable more accurate pose estimation for characterising the system's performance. Again, we emphasise that SLAM was run completely independently from the teach and repeat navigation, and was only used to measure performance. In particular we examine the effects on the system of inaccurate odometry, its sensitivity to parameter tuning and its robustness to low resolution images.

1) *Robustness to Odometry Errors*: Robustness to inaccurate odometry information was determined to be a key performance characteristic of the system, particularly for application to low cost robots for which no other self motion sensor information, such as an IMU, is available. Significant odometry variations were for example observed when operating robots on different floor surfaces, or as the tyre pressure dropped. As in [6], [24], orientation errors in odometry were found to be less critical, so here we examine the effects of an up to $\pm 30\%$ systematic artificial corruption of linear odometry measurements. Teach run odometry information was kept unchanged for all trials.

The results for 5 trials at each of the odometry corruption values is shown in Figures 5 and 6. Errors during the repeat runs were shown to increase gradually with increasing odometry errors and performance remained robust for the

TABLE II
SUCCESS RATE FOR DIFFERENT ODOMETRY CORRUPTION VALUES

Odometry	-30%	-20%	-10%	+0%	+10%	+20%	+30%
Success ours	0/5	5/5	5/5	5/5	5/5	5/5	0/5
Success Bearnav [6]	0/5	0/5	0/5	5/5	0/5	0/5	0/5

TABLE III
SUCCESS RATE FOR DIFFERENT CORRECTION GAINS

Orient. corr. gain K_θ	0	0.0001	0.001	0.01	0.1
Success	0/3	0/3	3/3	3/3	2/3
Along-path corr. gain K_p	0	0.0001	0.001	0.01	0.1
Success	3/3	3/3	3/3	3/3	0/3

range of $\pm 20\%$ corruption. Failures occurred for $\pm 30\%$ odometry error due to lateral path error exceeding the width of the corridors in which the robot was travelling. This result is in comparison to that presented for a similar teach and repeat approach in [24], which was only successful for -5% to $+10\%$ odometry error following a much simpler indoor route.

Additionally, we tested the Bearnav system [6] in the same conditions. It explicitly does not account for errors in odometry distance measurements, so served as a good benchmark to test the robustness improvement offered by our approach's along-path corrections. Indeed, Bearnav was successfully able to repeat the route with accurate odometry, but failed consistently for even $\pm 5\%$ odometry error.

2) Sensitivity Analysis of Teach Repeat Parameters:

A sweep of the teach repeat correction gain parameters was performed to establish the sensitivity of the system to calibration. The default value was empirically chosen to be 0.01 for both orientation and along-path correction and this was held constant for one correction while varying the other, assuming negligible interaction effects. The results in Table III show the system working over at least one order of magnitude for both of the corrections.

The system still worked without any path correction, but this was expected when compared to the successful repeat results for Bearnav which does not implement path correction. Over the distance of the indoor run, the Jackal's linear odometry accuracy was sufficient for path following.

To stress the importance of the path correction, we conducted additional experiments where we set $K_p = 0$ and artificially corrupted the linear odometry as in the previous experiment. In this case, the repeat runs fail consistently even for a relatively moderate corruption of $\pm 10\%$.

3) Robustness to Reduced Image Size: A further test of this approach was conducted to see the effects of running the system with low resolution images, motivated by the successful navigation strategies of ants with their limited visual systems [18], [19]. Fig. 7 shows results obtained using Miro on a short ($\approx 15\text{m}$) but challenging outdoor route with many obstacles and sharp turns. One can observe that our approach performs reliably with image resolutions as small

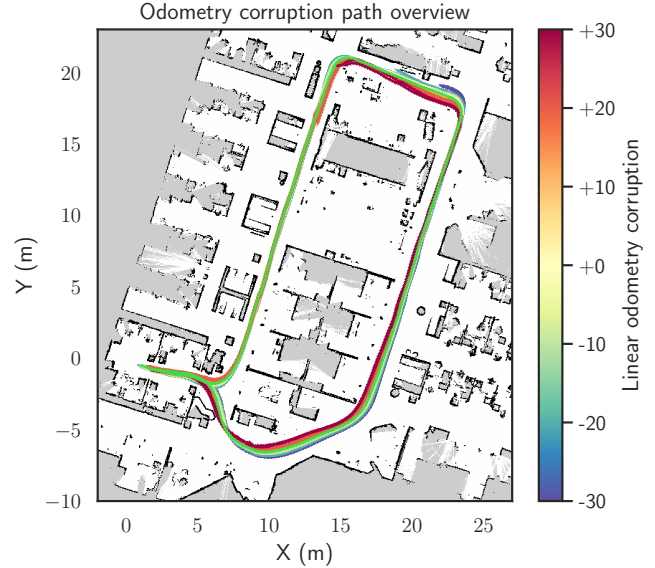


Fig. 5. Overview of the system's indoor traverses with corrupted odometry: One can observe increasing deviations from the teach run (green line) with increasing odometry corruption multiplier. Please refer to Fig. 6 for a quantitative analysis of these results.

as 23×8 , before performance degrades.

On the Jackal robot, we still had reliable performance using 57×22 images for the outdoor route (teach in bright sunlight, repeat overcast) and using 32×12 images indoors.

We generally observed that lower resolution images could be used successfully when visual conditions were similar between teach and repeat, but tended to fail when conditions changed.

C. Extension Test 1: Long Distance Outdoor Trials

A 550 m teach run was performed outdoors on the QUT university campus during bright sunny conditions. An overview of the run is shown in Figure 8. Challenges included high contrast shadows in the environment, and people walking past the robot. Four repeat runs were performed, all in overcast conditions and one a month after the teach run recording. One of the repeat runs was successfully performed with a reduced image resolution of 60×20 . We showcase these challenging conditions in our Multimedia Material.

D. Extension Test 2: Transferring Teach Run Between Robots

For this test, we recorded a teach run on the Miro platform along the same indoor route as in Figure 5. As shown in Figure 4, the Miro robot is much lower to the ground than the Jackal and has a wider field of view from its two wide angle cameras. Miro's odometry information is also much noisier than that of Jackal, and has a noticeable leftwards bias. The teach run was copied to the Jackal, the only modification being that the images were cropped to approximately match the Jackal's field of view. Parameters for the Jackal were kept the same as for the Miro, as in Table I, only the controller speed parameters were adjusted to account for the different dynamics of the two platforms.

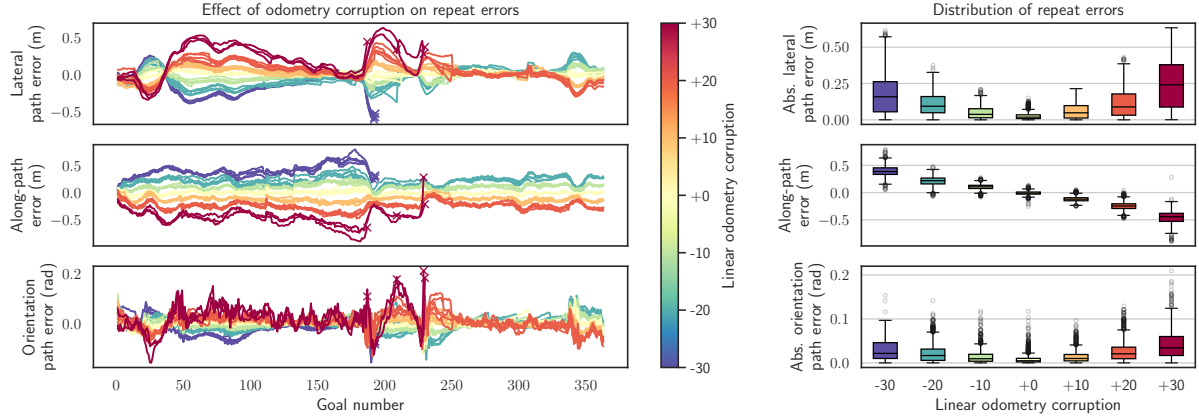


Fig. 6. System's robustness to corrupted linear odometry. One can observe that errors grow smoothly with increased linear odometry corruption, and that along-path errors are as expected for positive or negative odometry errors. The crosses indicate when the strongly corrupted odometry caused the navigation to fail during a run.

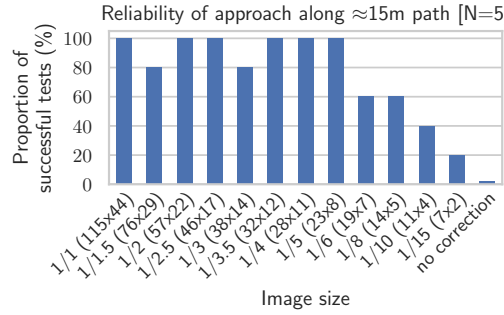


Fig. 7. System's robustness to low resolution images. Performance only drops significantly with image resolutions lower than 23×8 .

Despite a different camera with perspective shift and different odometry between the two robots, the Jackal successfully repeated the run taught to Miro. While previous teach repeat approaches have operated on different robotic platforms, such as in [6], [13], to the best of the authors' knowledge this is the first instance of a teach run being performed on one robotic platform, and successfully repeated on another. This demonstrates our approach's high robustness to viewpoint change and odometry information, and provides promise that the approach could be easily deployed on other robots as further discussed in the Conclusions.

E. Computational Analysis

The main computational bottleneck of the approach is in running the NCC search window over the image for each image in the search range. To achieve this in real time (15 Hz) onboard the Miro, which has a Raspberry Pi 3B+ computer, it was necessary to downscale the images and use a reduced along-path search range. As shown previously, the system continues to function successfully with these low resolution images. And there remains the potential for significant software optimisation. Despite this, our approach using low resolution images requires less computation than the state-of-the-art while performing more robustly to odometry errors thanks to the along-path correction (Table IV).

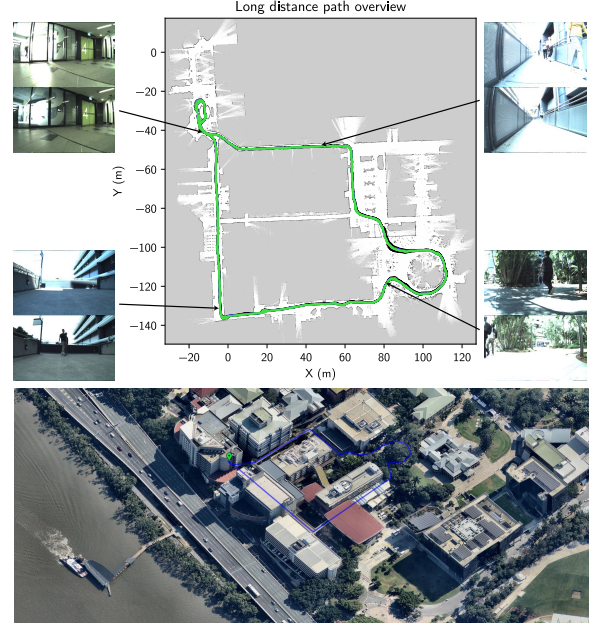


Fig. 8. Overview of the system's traverses outdoors. (Top) The teach run is shown in green, the three standard repeat runs in black, and the low resolution repeat run in blue. Major differences between teach and repeat are predominantly due to errors in the SLAM pose estimate, hence why no metric error analysis was performed for the outdoor trials. Example images of the teach and corresponding repeat runs at four exemplary points are shown to either side. (Bottom) Aerial view of the outdoor traverse (indicated with a blue line).

V. CONCLUSION

Visual teach and repeat has been an active research topic over the past two decades with applications ranging from a robot tour guide to interplanetary rovers. In this paper, we presented a novel teach and repeat approach that is particularly well suited for low-cost robots, as it can operate with a low-resolution monocular camera and noisy odometry information. We have demonstrated that our approach works indoors and outdoors on different robotic platforms without parameter adjustment. Our approach can efficiently utilise odometry information for navigation, while employing a periodic vision-

TABLE IV
COMPUTATION COMPARISON BETWEEN APPROACHES

Approach	Image processing (ms)	Full correction (ms)
Jackal ours: $115 \times 44 (K = 3)$	16	21
Miro ours: $29 \times 11 (K = 1)$	26	73
Jackal Bearnav: 640×480	25	28

based correction signal to remain robust to odometry errors.

Our approach has the following limitations: Firstly, in environments that have very few nearby visual features (e.g. a large open field), the correction signal is weak so we experience reduced metric accuracy. Essentially, our approach's accuracy scales with the environment's visual density – providing accuracy when needed. But the system could be augmented to also focus on ground textures, allowing greater metric accuracy in a wider range of environments. Secondly, our approach relies on rotational position offsets causing horizontal image offsets. This assumption could be violated in significantly non-flat environments, or when using a strongly distorted fish-eye camera. While we demonstrate navigation along a small incline in our Multimedia Material, a natural extension of this method would be to run a second stage of searching, using vertical sweeping or a mutual information metric, when the horizontal match correlation is too low.

One further research avenue is to track the system's confidence in its path following and slow down or trigger a recovery manoeuvre if confidence drops too low. There is also significant potential for offline preprocessing of the teach run images to enhance image features such as obstacles that are more important to match correctly. Furthermore, we would like to use our teach and repeat approach to cross-train navigation capabilities across robotic platforms. For example, one could obtain a navigation policy on the Jackal robot using a reinforcement learning approach, and then repeat the learned policy on the Miro robot. This is conceptually similar to the sim-to-real transfer problem, where it is well known that transferring policies is extremely challenging [35], [36].

REFERENCES

- [1] A. D. Ekstrom, "Why vision is important to how we navigate: Human Spatial Navigation and Vision," *Hippocampus*, vol. 25, no. 6, pp. 731–735, 2015.
- [2] F. Bonin-Font, A. Ortiz, and G. Oliver, "Visual Navigation for Mobile Robots: A Survey," *J. Intell. Robot. Syst.*, vol. 53, no. 3, pp. 263–296, 2008.
- [3] W. Burgard *et al.*, "Experiences with an interactive museum tour-guide robot," *Artif. Intell.*, vol. 114, no. 1-2, pp. 3–55, 1999.
- [4] D. Gallacher, "Drone Applications for Environmental Management in Urban Spaces: A Review," *Int. J. Sustain. Land Use Urban Planning*, vol. 3, no. 4, 2017.
- [5] J. Roberts *et al.*, "Autonomous control of underground mining vehicles using reactive navigation," in *IEEE Int. Conf. Robot. Autom.*, 2000, pp. 3790–3795.
- [6] T. Krajinik, F. Majer, L. Halodova, and T. Vintr, "Navigation without localisation: Reliable teach and repeat based on the convergence theorem," in *IEEE/RSJ Int. Conf. Intell. Robot. Syst.*, 2018, pp. 1657–1664.
- [7] M. Warren *et al.*, "There's No Place Like Home: Visual Teach and Repeat for Emergency Return of Multirotor UAVs During GPS Failure," *IEEE Robot. Autom. Lett.*, vol. 4, no. 1, pp. 161–168, 2019.
- [8] T. Nguyen, G. K. I. Mann, R. G. Gosine, and A. Vardy, "Appearance-Based Visual-Teach-And-Repeat Navigation Technique for Micro Aerial Vehicle," *J. Intell. Robot. Syst.*, vol. 84, no. 1-4, pp. 217–240, 2016.
- [9] P. Furgale and T. D. Barfoot, "Visual teach and repeat for long-range rover autonomy," *J. Field. Robot.*, vol. 27, no. 5, pp. 534–560, 2010.
- [10] T. Krajinik *et al.*, "Simple yet stable bearing-only navigation," *J. Field. Robot.*, vol. 27, no. 5, pp. 511–533, 2010.
- [11] S. R. Bista, P. R. Giordano, and F. Chaumette, "Appearance-based indoor navigation by IBVS using mutual information," in *Int. Conf. Control Automat. Robot. Vision*, 2016.
- [12] S. R. Bista, P. R. Giordano, and F. Chaumette, "Appearance-based Indoor Navigation by IBVS Using Line Segments," *IEEE Robot. Autom. Lett.*, vol. 1, no. 1, pp. 423–430, 2016.
- [13] S. R. Bista, P. R. Giordano, and F. Chaumette, "Combining line segments and points for appearance-based indoor navigation by image based visual servoing," in *IEEE/RSJ Int. Conf. Intell. Robot. Syst.*, 2017, pp. 2960–2967.
- [14] L. G. Camara *et al.*, "Accurate and Robust Teach and Repeat Navigation by Visual Place Recognition: A CNN Approach," in *IEEE/RSJ Int. Conf. Intell. Robot. Syst.*, 2020.
- [15] C. McManus, P. Furgale, B. Stenning, and T. D. Barfoot, "Visual Teach and Repeat using appearance-based lidar," in *IEEE Int. Conf. Robot. Autom.*, 2012, pp. 389–396.
- [16] L. Clement, J. Kelly, and T. D. Barfoot, "Robust Monocular Visual Teach and Repeat Aided by Local Ground Planarity and Color-constant Imagery," *J. Field. Robot.*, vol. 34, no. 1, pp. 74–97, 2017.
- [17] C. Cadena *et al.*, "Past, Present, and Future of Simultaneous Localization and Mapping: Toward the Robust-Perception Age," *IEEE Trans. Robot.*, vol. 32, no. 6, pp. 1309–1332, 2016.
- [18] T. S. Collett, "Landmark learning and guidance in insects," *Philos. Trans. R. Soc. B*, vol. 337, no. 1281, pp. 295–303, 1992.
- [19] J. Zeil, N. Boeddeker, and W. Stürzl, "Visual Homing in Insects and Robots," in *Flying Insects and Robots*, D. Floreano, J.-C. Zufferey, M. V. Srinivasan, and C. Ellington, Eds., 2009, pp. 87–100.
- [20] F. Labrosse, "Short and long-range visual navigation using warped panoramic images," *Robot. Auton. Syst.*, vol. 55, no. 9, pp. 675–684, 2007.
- [21] B. Webb, "The internal maps of insects," *J. Exp. Biol.*, vol. 222, 2019.
- [22] Y. Matsumoto, M. Inaba, and H. Inoue, "Visual navigation using view-sequenced route representation," in *IEEE Int. Conf. Robot. Autom.*, 1996, pp. 83–88.
- [23] D. Burschka and G. Hager, "Vision-based control of mobile robots," in *IEEE Int. Conf. Robot. Autom.*, 2001, pp. 1707–1713.
- [24] A. M. Zhang and L. Kleeman, "Robust Appearance Based Visual Route Following for Navigation in Large-scale Outdoor Environments," *Int. J. Robot. Res.*, vol. 28, no. 3, pp. 331–356, 2009.
- [25] P. Vandish, A. Vardy, and P. King, "Towards AUV Route Following Using Qualitative Navigation," in *Conf. Comput. Robot. Vision*, 2012, pp. 425–432.
- [26] P. King, B. Anstey, and A. Vardy, "Preliminary field trials of autonomous path following," in *IEEE Auton. Underwater Veh.*, 2014.
- [27] A. Dame and E. Marchand, "Using mutual information for appearance-based visual path following," *Robot. Auton. Syst.*, vol. 61, no. 3, pp. 259–270, 2013.
- [28] Z. Chen and S. Birchfield, "Qualitative vision-based mobile robot navigation," in *IEEE Int. Conf. Robot. Autom.*, 2006, pp. 2686–2692.
- [29] Z. Chen and S. Birchfield, "Qualitative Vision-Based Path Following," *IEEE Trans. Robot.*, vol. 25, no. 3, pp. 749–754, 2009.
- [30] S. Lowry *et al.*, "Visual Place Recognition: A Survey," *IEEE Trans. Robot.*, vol. 32, no. 1, pp. 1–19, 2016.
- [31] M. J. Milford and G. F. Wyeth, "SeqSLAM: Visual route-based navigation for sunny summer days and stormy winter nights," in *IEEE Int. Conf. Robot. Autom.*, 2012, pp. 1643–1649.
- [32] P. Corke, *Robotics, Vision and Control*, ser. Springer Tracts in Advanced Robotics, B. Siciliano and O. Khatib, Eds. Springer, 2011, vol. 73.
- [33] J. Lewis, "Fast Normalized Cross-Correlation," *Ind. Light & Magic*, vol. 10, 2001.
- [34] S. Macenski, "On Use of the SLAM Toolbox: A Fresh(er) look at Mapping and Localization for the Dynamic World," in *ROSCon*, 2019.
- [35] K. Rana *et al.*, "Multiplicative controller fusion: A hybrid navigation strategy for deployment in unknown environments," in *IEEE/RSJ Int. Conf. Intell. Robot. Syst.*, 2020.
- [36] P. Nguyen *et al.*, "Transferring Visuomotor Learning from Simulation to the Real World for Manipulation Tasks in a Humanoid Robot," in *IEEE/RSJ Int. Conf. Intell. Robot. Syst.*, 2018, pp. 6667–6674.